Numerical Investigation on the Deformational Behavior of Continuous Buried Pipelines Under Reverse Faulting

Amin Monshizadeh Naeen & Ehsan Seyedi Hosseininia

Arabian Journal for Science and Engineering

ISSN 2193-567X

Arab J Sci Eng
DOI 10.1007/s13369-020-04766-2

Springer

Arabian Journal for Science and Engineering
https://doi.org/10.1007/s13369-020-04766-2

RESEARCH ARTICLE-CIVIL ENGINEERING

Numerical Investigation on the Deformational Behavior of Continuous Buried Pipelines Under Reverse Faulting

Amin Monshizadeh Naeen[1] · **Ehsan Seyedi Hosseininia**[1]

Received: 13 February 2020 / Accepted: 1 July 2020

Abstract
Steel pipelines are vulnerable to the movements of active faults. Few studies focused on reverse faults. The deformational behavior of buried steel pipelines crossing an active reverse fault is investigated in this paper by applying 3D continuum finite element modeling. Numerical simulations indicate that local buckling (or wrinkling) mode of failure is more sensitive to the pipeline rather than tensile failure mode. The results were also confirmed by the experiment. Based on parametric studies, the pipeline capacity against failure can be significantly improved by reducing the burial depth and the pipe thickness ratio. Besides, the soil consistency around the pipe has a great effect on the behavior of buried pipelines. Furthermore, it is found out that the failed pipeline sections would be generated in longer distance from the fault plane as the soil behaves more softly or the pipeline is more flexible. These findings can lead the designers to have a safer and economic design of pipelines crossing reverse faulting zones.

Keywords Buried pipelines · Reverse fault · Geotechnical parameters · Numerical model

List of Symbols

c	Soil cohesion
C_c	Coefficient of curvature
C_u	Coefficient of uniformity
D	Pipe diameter
D_{50}	The average particle size of soil
E	Soil elastic Young's modulus
E_1	Elastic Young's modulus of pipe
E_2	Plastic Young's modulus of pipe
E_i	Initial Young's modulus of pipe in the Ramberg–Osgood stress–strain equation
f	Friction factor
G_s	Specific gravity
H	Burial depth of the pipeline
n	Ramberg–Osgood parameter
R	Pipe radius
r	Ramberg–Osgood parameter
t	Pipe wall thickness
β	Fault dip angle
δ	Interface angle of friction for pipe and soil
γ	Total unit weight of soil
γ_d	Dry unit weight of soil
ε_1	Initial yield strain of pipeline
ε_2	Failure strain of pipeline
ε_c	Compressive strain
ε_t	Tensile strain
ε_u	Ultimate strain
ε_a	Axial strain
μ	Coefficient of friction
ν	Poisson's ratio
σ_0	Effective yield stress
σ_1	Initial yield stress of pipeline
σ_2	Failure stress of pipeline
σ_a	Maximum axial stress
ϕ	Internal friction angle of soil
ψ	Dilation angle of soil

✉ Ehsan Seyedi Hosseininia
eseyedi@um.ac.ir

Amin Monshizadeh Naeen
amin.monshizadehnaeen@mail.um.ac.ir

[1] Department of Civil Engineering, Faculty of Engineering, Ferdowsi University of Mashhad, P.O. Box 91775-1111, Mashhad, Iran

1 Introduction

Failure of buried pipelines may occur because of natural events such as earthquake wave propagation and Permanent Ground Deformation (PGD). Previous investigations have proved that, unlike the surface structures, most of seismic

Published online: 16 July 2020

damages to pipelines were because of PGD such as fault movement, landslide, and liquefaction [1–3] and there were few cases that pipelines were damaged only by wave propagation [4, 5]. The experiences of damages caused by large fault displacements in strong earthquakes (e.g., the 1906 San Francisco earthquake, the 1995 Kobe earthquake, the 1971 San Fernando earthquake, the 1972 Managua earthquake, the 1976 Tangshan earthquake, the 1990 Manjil earthquake, the 1999 Chi–Chi earthquake, and the 1999 Izmit earthquake) are examples among others that clearly show the effect of large fault movements on pipeline failure [1, 4, 6–12].

Newmark and Hall [13] as the pioneers tried to predict the mechanical behavior of pipelines under fault movements. They assumed that during fault motion, the pipeline is under direct tension longitudinally and deforms axially between the effective anchor points. They discarded the lateral soil forces and the bending stiffness of the pipeline. Kennedy et al. [14] continued the work of Newmark and Hall [13] by considering the effect of lateral soil forces on the pipeline and associated bending strain. They also improved the modeling of longitudinal soil friction forces. A trial and error approach is used in Kennedy et al. [14] approach to determine axial stress that produces an axial elongation equal to the required elongation calculated basis of a specific fault displacement. The procedure ignores the bending stiffness of the pipeline [15]. Wang and Yeh [16] and Karamitros et al. [17, 18] introduced some refinements to existing analytical methods. Many researchers have also carried out centrifuge tests [8, 10, 19–21] or large-scale tests [22–24] on a buried pipeline to investigate the effect of various parameters such as faulting offset, burial depth, pipe-fault crossing angle, pipe diameter, etc., on the axial and bending strains of buried pipes. However, because of laboratory limitations, most of these experimental tests were focused on small fault displacement. In addition to analytical and experimental models, numerical methods provide researchers with the ability to carry out more detailed studies on various conditions of faults and pipelines. The evaluation of pipe bending strain under various geometric conditions [25, 26] and assessment of the behavior of continuous pipeline under the strike-slip fault [27] are some examples among the first attempts. Several numerical studies were also conducted in recent years using advanced finite element method. However, most of researches [28–36] have focused on a strike-slip fault with respect to the other types including reverse and normal faults. This is probably because of the comparatively easy modeling of the symmetric nature of strike-slip faulting. On the other hand, the lack of complete symmetry in the complex normal and reverse faulting has made the modeling more challenging. Therefore, less attention has been paid to the buried pipelines under normal [35, 37] and reverse fault movements [38, 39].

Two sets of three-dimensional (3D) continuum finite element models of a buried continuous steel pipeline crossing an active reverse fault are established in this study with giving special attention to the effect of the modeling approach on pipeline response. The first set of 3D continuum models corresponds to the simulation of a full-scale laboratory work performed by Jalali et al. [23] in which a pipeline with a limited length crossing a reverse fault was considered. The second set of the 3D models concerns the simulation of unanchored continuous steel pipelines which has been already analyzed by using a simplified beam-spring model by Joshi et al. [38]. The effects of various geotechnical parameters and geometric conditions on pipe response are discussed for such a reverse fault-crossing problem.

2 Finite Element Modeling

In the present paper, the finite element (FE) software ABAQUS [40] is employed to simulate the mechanical behavior of a continuous steel pipe under reverse fault displacement. The surrounding soil medium and the buried pipe are modeled by using eight-node reduced-integration continuum brick elements (type C3D8R) and four-node reduced-integration shell elements (type S4R), respectively, to simulate complicated deformational behavior of the soil and the pipe (including the distortions of the pipeline cross-section and pipe wall wrinkling phenomenon) and their interaction more precisely.

In the case of long-buried pipelines, the dimension of the numerical FE model should be large enough to avoid the influence of the boundary conditions and border points on the pipeline responses, unless the ends of the pipes are anchored in a specific length. For unanchored pipelines and according to previous experiences [17, 18, 30], several models with different dimensions should be considered to evaluate the effect of model dimension on the reaction forces in the boundaries and the strains caused in the pipeline.

For an unanchored long continuous pipeline, the required length in the numerical simulation is an important issue to correctly capture the mechanical behavior of the pipeline. In this section, the mesh generation of a continuous pipeline with a diameter of 914.4 mm and a thickness of 12.7 mm buried inside the soil medium is explained. The introduced pipeline characteristics belong to the pipeline already analyzed by Joshi et al. [38] using a simplified beam-spring model. The pipeline is aimed to be deformed by a reverse fault crossing the middle of the pipeline with a high level of displacement up to 4 m. For the soil medium around the pipe, a cross-section of 10 m × 10 m is considered. To find the appropriate length, several numerical simulations are required by trial and error such that the effects of boundaries on the pipeline behavior are almost negligible. The results of

several analyses showed that in a model with a total length of 1200 m, the maximum values of strain and the location of the strain concentration occur within the 10 m distance on each side of the fault plane and these values gradually decline so that from the 20 m distance of each side of the fault plane, the change is minimized. Therefore, the 1200 m length of the pipeline and the soil medium was divided into several parts, as demonstrated in Fig. 1. In order to determine the element sizes of each part, several trial runs and sensitivity analyses were conducted. In each run, the size of the elements was adopted smaller and the value of the pipe strain was compared with that of the previous run until the changes in strain values become less than 10 to 15%. In the soil cross-section, smaller elements are used near the pipeline and the pipe cross-section is divided into 40 equal parts based on the mesh sensitivity analysis.

In this work, the explicit dynamic analysis is used to simulate the quasi-static condition of a moving fault problem. This analysis method prevents the occurrence of convergence problems, which usually occurs in other analyses like implicit-dynamic and general-static in the post-buckling analyses. This sort of analysis is computationally efficient for the analysis of large models associated with large deformation and models with a high degree of nonlinearity [40].

To simulate fault movement, the soil mass is divided into two similar blocks: one of them is fixed and the other one moves toward the fixed part to simulate the fault displacement with a specific dip angle. To provide the quasi-static analysis condition, the fault displacement is implemented gradually and smoothly to inhibit the impact of inertia and dynamic forces on the pipeline response. On the other hand, an excessively large loading duration increases the computational time substantially. According to the ABAQUS manual [40], if the kinetic energy of the model does not exceed a small fraction (typically 5% to 10%) of its internal energy throughout the analysis, the simulation is assumed to be run quasi-statically [40]. Figure 2 shows the time variation of kinetic energy (KE) and internal energy (IE) for the benchmark soil model (dense sand in Table 6). The quantity of kinetic energy is less than 5% of the internal energy during fault movement, which confirms the finite

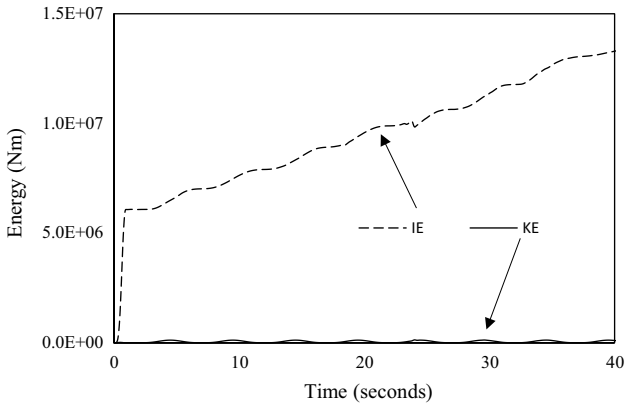

Fig. 2 Time variation of kinetic energy (KE) and internal energy (IE) of the model for the benchmark sand

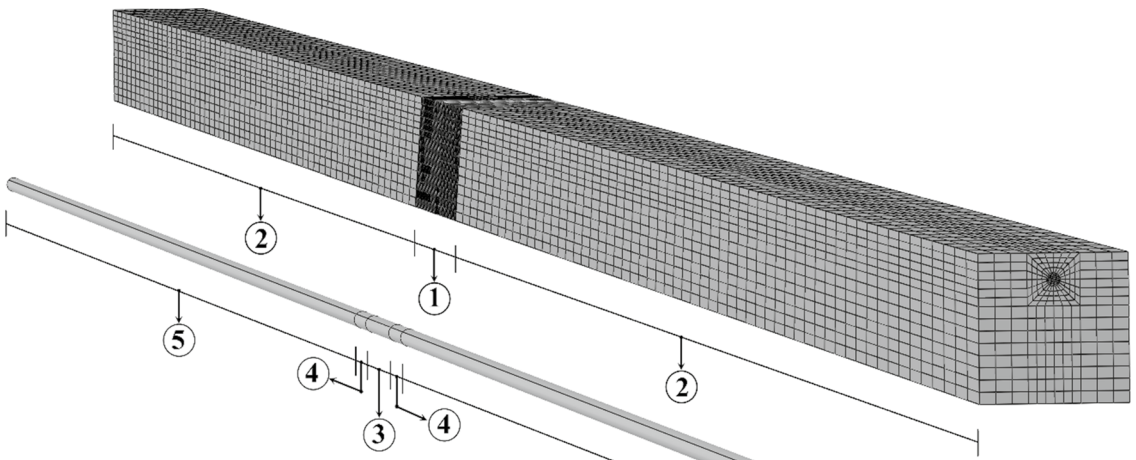

	Section				
	1	2	3	4	5
Partition Length (m)	60	570	30	15	570
Element Length (m)	1	10	0.25	0.5	2.5

Fig. 1 Division, dimensions and meshing style of the 3D mode

element simulations were indeed unexcited during fault displacement.

The analysis is conducted in two steps as follows: In the first step, the gravity loading is applied to the whole model to account for the initial stress state. In the next step, the fault displacement is exerted on the sides and the bottom boundaries of the moving block. The bottom and vertical boundaries of the fixed block are restrained in all directions. To provide static equilibrium or stability of the pipeline, it is essential to provide zero relative displacement between the nodes at the ends of the pipe and the nodes of the adjacent soil. For this purpose, the nodes at the ends of the pipe in the moving block were displaced in the same way as the side nodes of the moving block, and the nodes at the ends of the pipe in the fixed block were constrained in all directions.

As for the soil constitutive model, a linear elastic—perfectly plastic model with Mohr–Coulomb failure criterion is implemented with the parameters of cohesion (c), internal friction angle (ϕ), elastic modulus (E), dilatancy (ψ), and Poisson's ratio (ν). The soil behavior in simulations can be either considered as drained or undrained by choosing appropriate values of the soil parameters. It is noted that the soil condition is often drained since granular soil is used in practice around the pipeline and the fault displacement rate might be so small that the saturated fine-grained soil would behave in drained condition too.

To model the interaction between the pipeline and the soil, the ABAQUS automated surface-to-surface contact option has been used. The frictional behavior of contacting surfaces is calculated based on the concept of the Coulomb friction law in which the slippage of two contacting bodies relates to the frictional resistance over the interface surface defined by multiplying the contact pressure and the friction coefficient (μ) of the contacting surface [40]. The friction coefficient is $\mu = \tan(\delta)$ where δ is the friction angle of the interface between the soil and the pipeline and is defined as $\delta = f \times \phi$ in which f is the pipe coating factor. In the present paper, by assuming a rough steel surface for the pipeline without any special coating, $f = 0.8$ is chosen if it is in contact with granular soils [41]. For cohesive soils, $\mu = 0.3$ is adopted based on the suggestions mentioned in previous studies [33, 34]. It is also mentioned that the gap formation (separation after contact) is allowed in the model. In the simulations, the internal pressure of the pipeline is not considered.

3 Verification

According to the explanations mentioned above, a numerical model is constructed in order to be validated and the results are compared with those obtained by an experimental model performed by Jalali et al. [23]. Unlike small scale or centrifuge models, Jalali et al. [23] carried out a full-scale laboratory test to study the behavior of buried API-5L Grade B pipeline under reverse fault movement. The physical model includes a soil box with a cross-section of 2 m high and 1.7 m wide and a crossing pipeline with a length of 8 m. The tested steel pipeline has a stress–strain relationship according to the following equation which calculates the axial strain (ε_a) based on Ramberg–Osgood formulation of pipeline material [42]:

$$\varepsilon_a = \frac{\sigma_a}{E_i}\left[1 + \frac{n}{(r+1)}\left(\frac{\sigma_a}{\sigma_0}\right)^r\right] \quad (1)$$

where σ_a is maximum axial stress, E_i is the initial Young's modulus of the pipe, σ_0 is the effective yield stress, r and n are Ramberg–Osgood parameters presented in Table 1. The stress–strain curve of the API-5L Grade B is shown graphically in Fig. 3. It is noted that in the simulations, the maximum principal in-plane stress/strain component of the shell elements is considered as the axial stress/strain value corresponding to this constitutive model.

The geometric conditions of the experiment (H: burial depth, t: thickness, D: diameter) and the properties of the soil are shown in Tables 2 and 3, respectively. The burial depth (H) in the Jalali et al.'s experiment [23] was measured from the center of the pipeline.

As for the numerical model, the same size as the laboratory setup is considered. The element size and loading rate are chosen based on the same methodology described in Sect. 2. The size of the soil medium and the pipeline along its length is set to 15 mm and 10 mm, respectively, and the pipe cross-section is divided into 16 equal parts. Also, the

Table 1 Parameters of the Ramberg–Osgood stress–strain relationship for API-5L grade B steel pipe [43]

E_i (MPa)	σ_0(MPa)	n	r
210,000	320	17.896	9.3

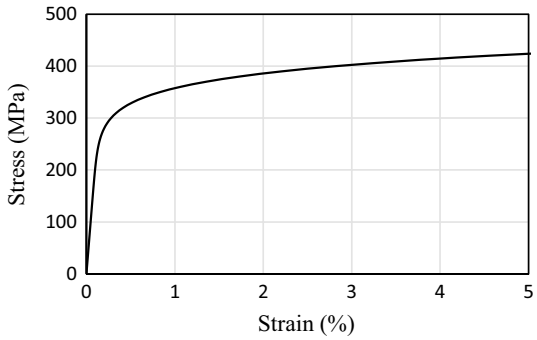

Fig. 3 Stress-strain curve of the API-5L Grade B

Table 2 Properties of the experimental tests by Jalali et al. [23]

Model dimensions (m)	Fault displacement (mm)	Fault dip angle (°)	*H*/*D*	*H* (m)	*D*/*t*	*T* (mm)	*D* (mm)
2×1.7×8	600	61	8.8	1	26	4.4	114.3

Table 3 Material properties for sand backfill used in the experimental tests [23]

C_c, coefficient of curvature	1.01
C_u, coefficient of uniformity	6.69
D_{50}, average particle size (mm)	1.1
ϕ, friction angle (°)	33.5
ψ, dilation angle (°)	0
c, cohesion (kPa)	5
G_s, specific gravity	2.56
γ_d, dry unit weight (kN/m^3)	17.9

loading duration of 5 s is adopted to establish a quasi-static condition in the analysis. In the numerical simulation, the Ramberg–Osgood and Mohr–Coulomb constitutive models were dedicated to the pipe and soil, respectively, with the parameters introduced in Tables 1 and 2.

The longitudinal strains at the crown and the invert of the pipeline for various magnitudes of ground displacement for both the numerical and experimental models together with the relative error are illustrated in Fig. 4. Tensile and compressive strains are defined in positive and negative signs, respectively. According to Fig. 4a, b, the value of the peak compressive strain at the invert of the pipe is higher than that of the crown, while the magnitude of peak tensile strains at both crown and invert of the pipeline is almost equal. The maximum changes in the strain values occur within the distance of 1.5 m on each side of the fault trace. For the distance of over 2 m (or more than $17.5 \times D$), the effect of faulting on the pipeline is almost negligible. These observed trends are similar for both numerical and experimental models. The relative error for peak values of compressive as well as tensile strains of the numerical method compared to the experimental model is illustrated in Fig. 4c for the crown and the invert of the

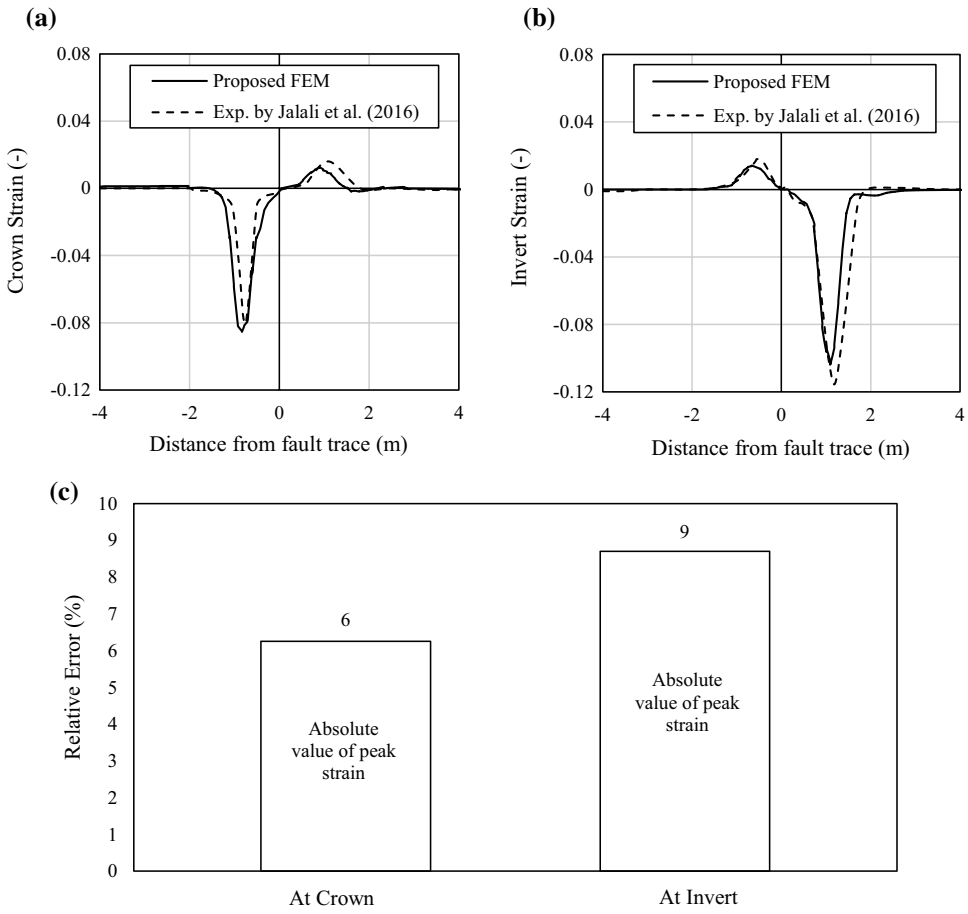

Fig. 4 Variations of the longitudinal strain at **a** crown and **b** invert of the pipeline, and **c** relative error of the numerical simulation

pipeline. The relative error for peak values of strains of the numerical method compared to the experimental model is illustrated in Fig. 4c for the crown and the invert of the pipeline. The relative error is defined as the difference of the maximum strains of the two models divided by that obtained in the experimental method. The error of the proposed FE method is less than 9% for the absolute value of peak strain. Therefore, there is good accordance between the experimental and numerical results, which confirms the validity of the proposed FE model. It is here noted that the differences observed in the results might be because of the difference in the loading (offset) rate which was not mentioned in the Jalali et al.'s [23] work, while this issue can influence numerical results because of dynamic or inertial effects. Another reason for the observed difference in strain values is probably due to the soil preparation method used in the experimental setup (split-box), which might be different from the soil sample in a direct shear test by which, the geotechnical parameters was measured.

4 Continuum FE Model Versus Beam–Spring Model

The accuracy in the simulation of the deformational behavior of pipelines buried in the soil depends on the simulation approach. In order to capture the accepted deformation pattern in the pipeline, a proper numerical approach should be implemented. It is worth mentioning that the main failure modes of continuous pipelines include the tensile failure and local buckling (or wrinkling) [9], which are caused due to axial tension and axial compression, respectively. If the pipeline is buried in sallow depth, it can also exhibit beam-buckling behavior under axial compression [9]. Beam buckling of a pipeline is similar to Euler buckling of a slender column in which the pipe undergoes a transverse upward displacement. The relative displacement is distributed over a large distance and hence, the magnitude of compressive pipe strains is not large. In compression zones, the beam buckling of a pipeline is not associated with the pipe failure and it may be better described as a serviceability problem. Rather, the local buckling may be considered as the main reason to cause the pipe to fail.

In the local buckling failure, after the initiation of the local pipe wall wrinkling, all further geometric distortion caused by ground deformation tends to concentrate at the wrinkling zone, which results in large deformations in the pipe wall and often leads to high levels of strain. Based on the ASCE Guidelines for the seismic design of oil and gas pipeline systems [15], the initiation of local buckling, i.e., the onset of wrinkling, occurs at a strain of 1/3 to 1/4 of the theoretical value of axial compressive strain (ε_c) defined as:

$$\varepsilon_c = 0.6 \times t/R \tag{2}$$

where t is the pipe wall thickness and R is the pipeline radius. IITK-GSDMA Guideline [44] suggests a value range for the allowable wrinkling strain. Hence, in terms of failure criterion, the onset of wrinkling is initiated if the pipe strain exceeds the axial compressive strain (ε_c):

$$\varepsilon_c = 0.175 \times t/R \tag{3}$$

The strain associated with tensile failure (ε_t) also ranges from 0.015 to 0.05 based on different guidelines [9, 41, 45–48].

According to American Lifeline Association (ALA) guidelines for the design of buried steel pipe [41], a pipeline may remain in service after the ovalization of the pipe cross-section, which denotes the distortion of the cross-section to an oval shape. However, the compressive and tensile strains should be limited to $\varepsilon_c = 1.76$ t/D and $\varepsilon_t = 0.04$, respectively, in order to meet the pressure integrity limit. Pressure integrity strain limit assumes that significant pipeline distortion is possible and pipeline repair or replacement would be required to return the pipe to normal service.

In this paper, the compressive and tensile strain limits introduced by ALA [41] ($\varepsilon_c = 1.76\ t/D$ and $\varepsilon_t = 0.04$) are considered as the criteria for the desired level of the pipeline serviceability. It is assumed that local buckling (or wrinkling) and tension failure would initiate if the maximum compressive and tensile strains occurring in the pipeline at any location exceed these allowable values. The ultimate value of true strain $\varepsilon_u = 0.8$ is considered as the ductile rupture limit [49] and the pipeline behavior is studied to this ultimate value if accessible.

In this section, the behavior of a buried pipeline against reverse fault movement is investigated by using two approaches including continuous FE and beam–spring methods. To this aim, a comparison is made between the results obtained from the current FE model and those from the beam-spring model presented by Joshi et al. [38]. Based on the Kennedy's method as explained briefly in the Introduction section, Joshi et al. [38] developed a simple FE model by using beam elements and nonlinear springs instead of the pipeline and the surrounding soil, respectively. In this approach, the pipeline-soil interaction is modeled by connecting the pipe nodes to a set of nonlinear springs in three perpendicular directions which are located at specific distances from each other. By this discretized concept, the pipe-soil interaction is not simulated continuously. However, the surface-to-surface contact method is applied in the FE approach which provides the ability to model the pipe-soil interaction without any gap. It is also noted that in the continuum modeling approach,

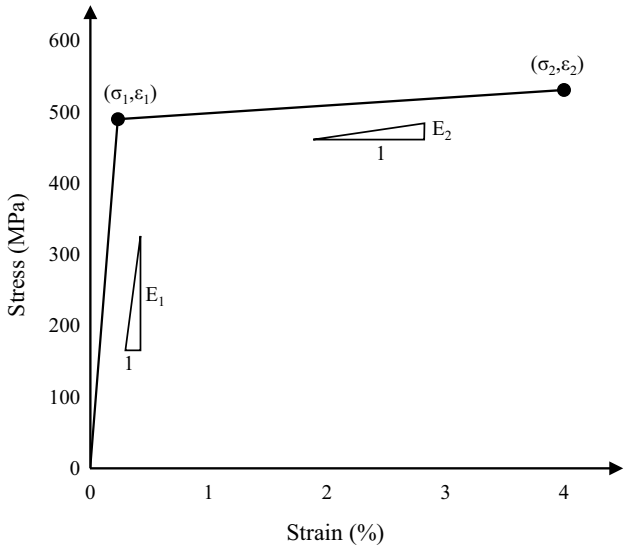

Fig. 5 The bilinear stress–strain relationship for the API-X65 steel

Table 4 API-X65 steel properties [18]

Initial yield stress (σ_1)	Failure stress (σ_2)	Failure strain (ε_2)	Elastic Young's modulus (E_1)	Initial yield strain (ε_1)	Plastic Young's modulus (E_2)
490 MPa	531 MPa	4.0%	210 GPa	0.233%	1.088 GPa

it is possible to take into account the initial stress state of the medium which is more realistic for the actual situation.

According to the procedure explained in Sect. 2, an API5L-X65 grade steel [50] pipeline with diameter $D=914.4$ mm (36 in.), thickness $t=12.7$ mm (0.5 in.) and a bilinear stress–strain curve is assumed to be buried at the depth of 1.75 m in a sandy soil with the internal friction angle $\phi=35^{\circ}$, the unit weight $\gamma=18$ kN/m^3, and the friction factor $f=0.8$. The bilinear stress–strain curve of the X65 steel material and its corresponding parameters are illustrated in Fig. 5 and Table 4, respectively.

For the current situation (i.e., $D=914.4$ mm and $t=12.7$ mm), the pipe would wrinkle at the strain level equal to -0.024 according to the onset of the wrinkling limit $\varepsilon_c=1.76\ t/D$. Figure 6 shows the variation of the maximum total compressive strain in the pipeline with the fault displacement for different fault dip angles $\beta=40^{\circ}$ and 70°. Comparison of the results with $\beta=40^{\circ}$ and $\beta=70^{\circ}$ in Fig. 6a, b, respectively, demonstrates that the strain values in the fault with dip angle $\beta=70^{\circ}$ are much less than those in the fault with dip angle $\beta=40^{\circ}$, for the same level of fault displacement. This is because of the influence of the fault dip angle on the deformation pattern of the pipeline. In fact, as the dip angle of the fault is smaller, the deformation of the pipe section is more severe, and consequently, the level of the maximum compressive strain increases. Consequently, the pipeline fails (or wrinkles) at a lower magnitude of fault displacement. Therefore, the difference in the results of the two modeling approaches becomes apparent at a lower magnitude of fault movement as the fault dip angle declines. It is clear that the value of maximum compressive strain in both continuum and beam-spring models has exceeded the onset of wrinkling limit, indicating the occurrence of local buckling of the pipe cross-section. In small fault movements, where the compressive strain level is low (less than -0.05), there is good accordance between the results of the two modeling approaches. However, by increasing the fault displacement, some discrepancies arise between the results. This is because the beam elements cannot simulate the local buckling (wrinkling) phenomenon, while this phenomenon can affect the pipe deformation pattern and the values of strain. This shortcoming is investigated and discussed by Sreenath et al. [51] and Sarawit et al. [52]. Furthermore, it is noted that, according to O'Rourke and Liu [9], local buckling is the main mode of the pipeline failure under compressive forces and the pipeline cross-section is extremely prone to experience local buckling during the reverse fault displacement. Therefore, the results obtained from the beam-spring method are not reliable, especially in large fault displacement magnitude. Based on the works of Sreenath et al. [51]

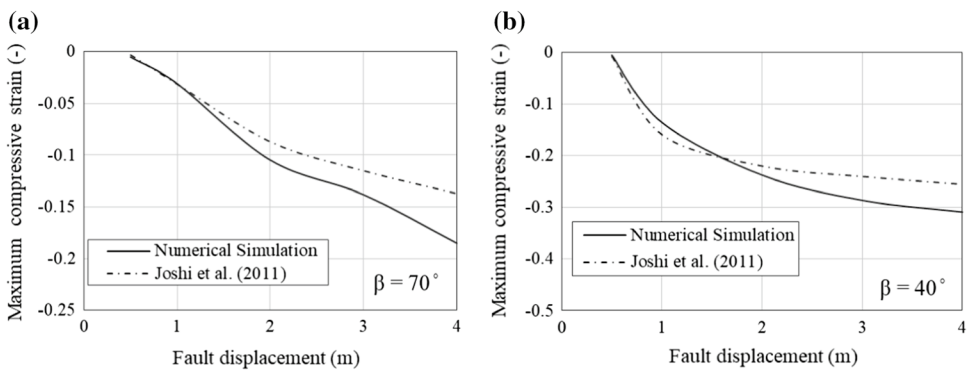

Fig. 6 Variations of the maximum compressive strain exerted in the pipe for the dip angle β **a** 40° **b** 70°

and Sarawit et al. [52], the S4R elements used in the presented model can properly simulate local buckling behavior.

5 Parametric Studies on the Behavior of Buried Pipelines

The response of a buried pipeline against a reverse fault displacement is investigated under various geotechnical and geometric conditions. To this aim, the effect of several soil parameters including cohesion (c), friction angle (ϕ), Young's modulus (E), and dilation angle (ψ) are considered. Furthermore, the effect of the buried pipe geometry on the pipe response is investigated by considering various burial depths (H) and the ratio of the diameter (D) to the pipe thickness (t). The results of the parametric study are presented in the following sections. For simplifying the simulations, it is assumed that the backfill soil has similar properties to the undisturbed surrounding soil. The total displacement of 2 m to 4 m is considered in the numerical simulation. Similar to the work of Joshi et al. [38], the burial depth is considered to the top of the pipe in the following subsections.

5.1 Effect of Cohesive Soils on Pipeline Response

To evaluate the effect of cohesive soils on pipeline response under the displacement of a reverse fault with the dip angle $\beta = 40°$, two types of soft clay and stiff clay are considered for the soil medium. An API-X65 steel pipe with diameter $D = 914.4$ mm (36 in.), thickness $t = 12.7$ mm (0.5 in.), and burial depth $H = 1.75$ m is assumed for the analysis. The soil properties under undrained loading condition are listed in Table 5.

The variation of maximum compressive, as well as tensile strains of the pipeline caused by reverse faulting, is presented in Fig. 7 for the two different cohesive soils. Generally, by increasing the fault displacement, both tensile and compressive strains rise. The growth rate of the strains until the displacement of 2 m is high, but in larger displacements, the strain change gradient is mild and almost constant. This behavior is probably because of the way of the pipe deformation. In fact, by the increase in the fault displacement, more length of the pipeline gets into plastic deformation (refer to Fig. 8) instead of strain concentration in a single element, and therefore, the magnitude of the maximum compressive strain does not climb anymore. Also, it is obvious that the magnitude of the compressive strain is much higher than that of the tensile strain and the pipeline exceeds the wrinkling failure limit (i.e., $\varepsilon_c = -0.024$) at a lower magnitude of fault displacement compared to displacement for the tensile failure limit (i.e., $\varepsilon_t = 0.04$). It is reminded that these limits are considered as serviceability limits which are explained before in Sect. 4. In the values of strain greater than ε_c and ε_t, the pipeline loses its functionality and is out of service. Therefore, the compressive strain is more critical and the possibility of the pipeline failure mode due to local buckling is more than that of the tensile failure mode. This trend is also observed in all other cases mentioned in the following sections. The results also demonstrate that the pipeline in the softer clay can move easier and therefore, lower interaction force is imposed on the pipeline surface, which results in a considerable reduction in the value of the strain. For instance, at the end of fault displacement, maximum compressive strain in the stiff clay is almost three times greater than that in the soft clay, while such an increasing effect is about 40% for the maximum tensile strain.

Table 5 Mohr-Coulomb parameters of clayey soils

	γ (kN/m^3)	E (MPa)	ψ (°)	ϕ (°)	C (kPa)	ν
Stiff clay	18	100	0	0	200	0.49
Soft clay	18	25	0	0	50	0.49

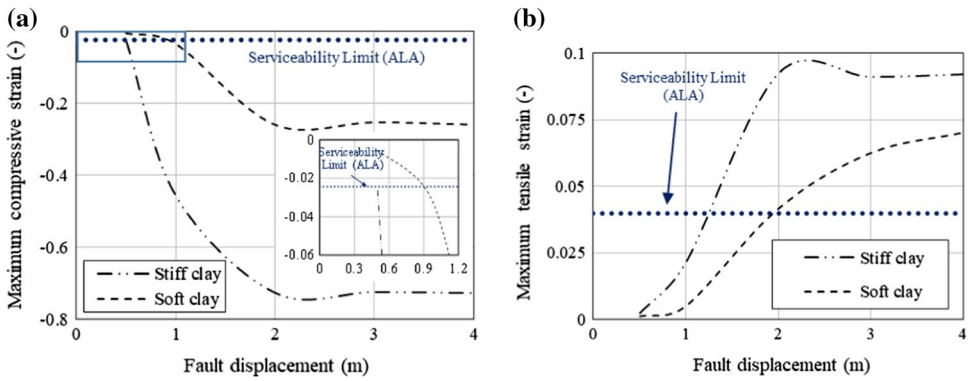

Fig. 7 Variation of pipeline strains with fault movement in different cohesive soils **a** maximum compressive strain **b** maximum tensile strain

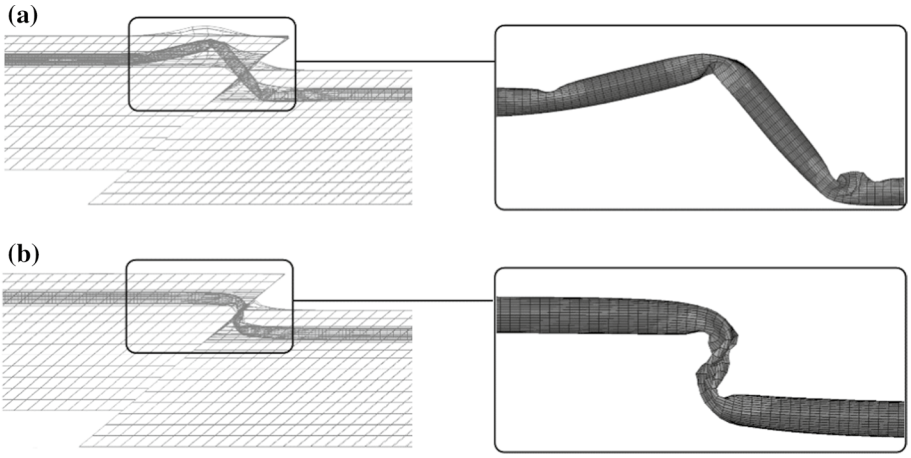

Fig. 8 Pipe deformation in **a** soft clay and **b** stiff clay

The deformed shape of the pipeline buried in the cohesive soils is illustrated in Fig. 8. It is seen that the pipeline in the soft clay displaces the upside soil and therefore, less pressure is imposed on the pipeline from the surrounding soil in comparison with the pipeline buried in stiff clay. It is also clear that the pipeline deformation pattern for the two different cohesive soils varies from each other. Actually, in stiff clay, the pipe failure occurs at the intersection point of the pipeline and the fault plane, while in the soft clay, the location of the pipe failure is far from the fault plane.

5.2 Effect of Cohesionless Soils on Pipeline Response

To investigate the effect of granular soils on pipeline behavior, a granular soil (e.g., sand) with three degrees of compaction (loose, medium dense, and dense) is considered. The geometric condition of the model is similar to the previous model described in the last section. The properties of the granular soils are listed in Table 6. Regarding the soil parameters selection, it is noted that the main attention is paid on the soil stiffness as well as the internal friction angle, which are more sensitive to the soil density and they have a wide range of values in different soil compaction degrees. To compare the effectiveness of these two parameters, the same value is adopted for other parameters. Because of the shallow burial depth, the unit weight has a very slight effect on the in situ stress states. A slight cohesion is considered for the soils in order to avoid the convergence issue in numerical simulations at large deformations in addition to the consideration of the actual small cohesion in the presence of clay in natural sandy deposits. The soil dilation angle is assumed to be zero and independent of the friction angle since the soil experiences a large deformation level (with fault displacement up to 4 m) at which, the critical state reaches. In Sect. 5.4, the effect of the soil dilatancy angle on the pipeline response is studied and explained. The values of the parameters are chosen based on practical values mentioned in geotechnical engineering references in the literature.

The variation of the maximum compressive and tensile strains is illustrated in Fig. 9. Similar to the case of cohesive soils described above, the increase in the fault displacement causes to augment the maximum tensile and compressive strains. The gradient of the strain changes decreases in the fault displacement larger than 2 m, especially for the compressive strain. Regarding the effect of soil compaction, it can be claimed that the maximum compressive strain increases with the soil compaction, while its effect on the maximum tensile strain is not so impressive. This behavior is probably because of the less limited deformation of the pipeline in lower compacted soils, which results in lower resistance (frictional) forces in the contact surface between the soil and the pipe.

Based on the serviceability (failure) limits of strains defined by ALA [41] as shown in Fig. 9, it is seen that the pipelines are primarily damaged in compression mode since the functionality in compressive limit strain is halted for the fault displacement less than one meter while the tensile failure occurs at around the fault displacement of 2 m. The

Table 6 Mohr-Coulomb parameters of sandy soils

	γ (kN/m^3)	E (MPa)	ψ (°)	ϕ (°)	C (kPa)	ν
Loose sand	18	10	0	30	5	0.3
Medium dense sand	18	45	0	35	5	0.3
Dense sand	18	75	0	45	5	0.3

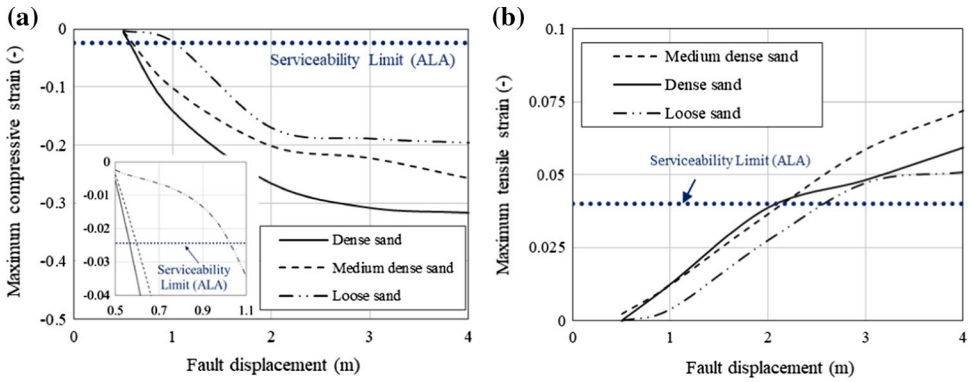

Fig. 9 Variation of pipeline strains with fault displacement for different granular soils **a** maximum compressive strain **b** maximum tensile strain

damage to the pipeline can be reduced if the compaction of the surrounded soil decreases which is more effective for the compressive part of the pipeline.

The pipeline deformation with different soil compaction states is demonstrated in Fig. 10. The overall deformation pattern of the pipelines is almost similar to each other and the wrinkle sections are generated far from the fault plane. However, as the soil compaction increases, more severe deformation occurs in the pipeline especially for the buried section in the footwall. This means that the pipe would lose its functionality sooner as the compaction increases.

In order to have a better scheme on the effect of soil type on the pipeline response, the maximum compressive strain of the pipe and the deformed shape of the pipeline are summarized in Fig. 11 for various types of cohesive and cohesionless soils. As shown in Fig. 11a, the minimum value of the pipeline strain occurs where the pipeline is buried in the loose sand, while the maximum compressive strain happens if the pipeline is buried in the stiff clay. The effectiveness of using low-density soil around the pipe can be easily seen in the graph. It can be figured out that the pipe would keep its serviceability in loose sand with the fault displacement up to 1 m, while the pipeline fails in compression with smaller fault displacement of 0.5 m if it is surrounded by dense sand (or stiff clay). Figure 11b also shows the deformed shape of the pipeline for various types of cohesive and granular soils. The deformation pattern of the pipeline in soft clay is similar to that of sandy soils, and three main failure points (local buckling) are observed along the pipeline. Nevertheless, the deformation pattern of the pipeline in stiff clay considerably differs from other types of the soils, and the pipeline has been failed only at one location of the intersection point

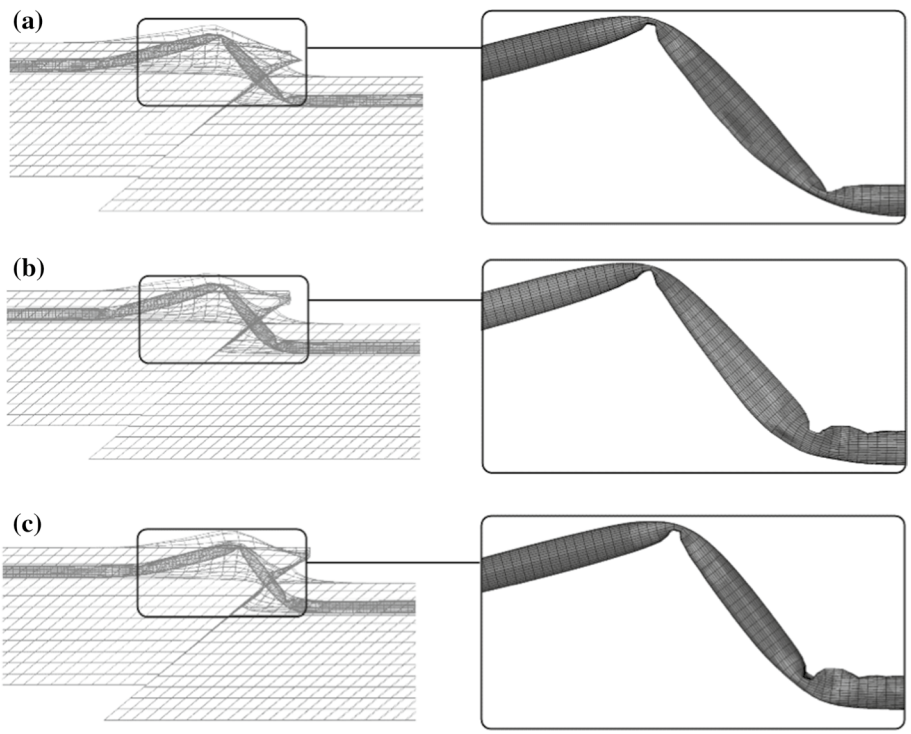

Fig. 10 Pipe deformation in **a** loose sand, **b** medium dense sand and **c** dense sand

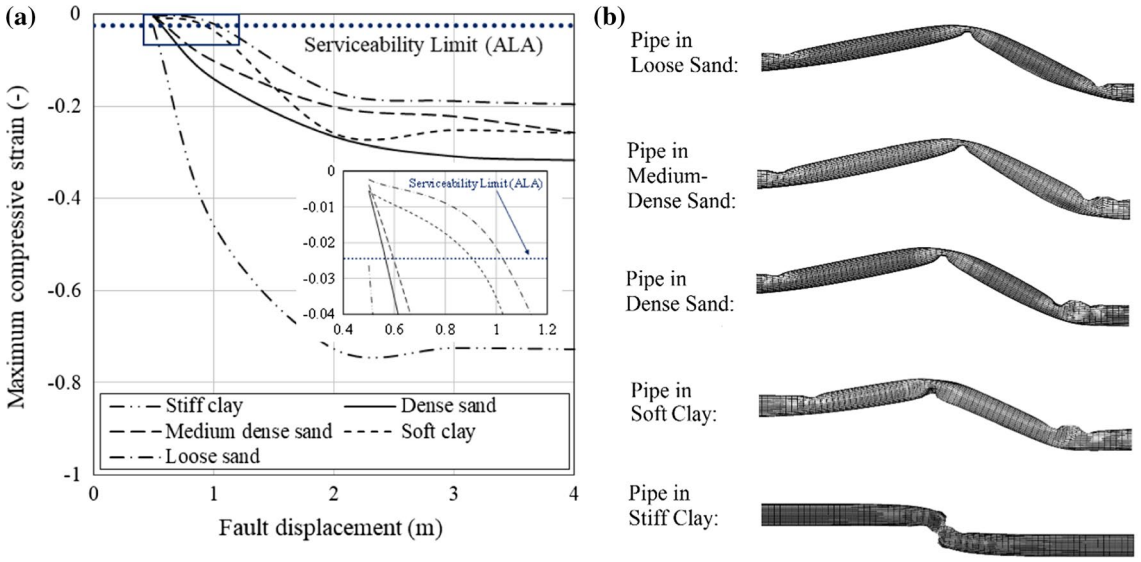

Fig. 11 The effect of soil types on **a** the maximum compressive strain in the pipe and **b** the deformation of buried pipes

of the fault plane and the pipeline, and the rest of the pipe has remained almost rigid. This can be justified in such a way that after the onset of wrinkling at the fault-pipeline intersection point, the high values of the cohesion and stiffness of the stiff clay prevent the free deformation of the pipeline, which results in further distortion at the wrinkle zone and consequently, the values of strains are considerably intensified. In other soil types, after the onset of wrinkling, however, the pipeline begins to bend at the vicinity of the buckled zone and therefore, the applied forces would expand around the buckled zone and the values of strains will decline.

5.3 Effect of Soil Stiffness on the Pipeline Response

To evaluate the effect of soil stiffness as an individual parameter on the response of buried pipelines, the dense sand in Table 6 is chosen as a benchmark with three different values of elastic modulus $E = 75$, 55, and 35 MPa. Figure 12a, b shows the maximum compressive and tensile strains for various values of E, respectively. It is seen that the change in the soil stiffness value has almost no effect on the value of the pipe compressive strain for the different levels of fault displacement. The increase in E has lowered the tensile strain slightly. By comparing Fig. 9a, b, it is obvious that the local buckling initially occurs at the pipe section at a small fault displacement (around 0.5 m) followed by tensile failure which occurs at bigger fault displacements (about 1.5–2 m). By comparing the results obtained in Figs. 9 and 12, it can be inferred that the more effective factor in determining the behavior of the buried pipeline in granular soils is the ϕ parameter. This is due to the effect of soil friction angle on the coefficient of friction (μ) and the related interaction forces along the soil and the pipeline surface.

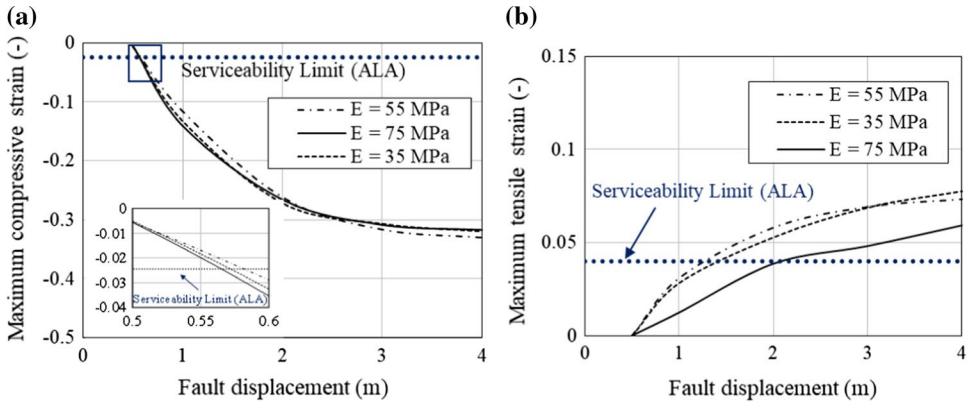

Fig. 12 The effect of soil stiffness on the pipe strain **a** maximum compressive strain and **b** maximum tensile strain

5.4 Effect of Soil Dilation Angle on Pipeline Response

Soil dilatancy denotes the expansion of soil volume under shear loading. Soil dilatancy is dependent on the soil relative density, confining stress level, and particle angularity. For the pipelines which are buried in shallow depths and the surrounded soil are nearly compacted, the particle angularity can be considered as the main influencing parameter on the manifestation of soil dilatancy. The more the soil particles are angular, the greater the dilatancy of the soil is. On the other hand, it is important to note that the soil dilatancy mostly appears at medium soil deformation levels, while the soil tends to have contractive behavior and zero dilation at small and large deformation levels, respectively. To evaluate the effect of soil dilatancy on the pipeline behavior for medium deformation levels (up to the fault displacement of 2 m), four dilation angles $\psi = 0$, 10, 20, and 30 degrees are considered for the benchmark case, i.e., the dense sand in Table 6. The value of the friction angle is assumed to be the same for all the soil cases. It is reminded that the peak friction angle increases with the dilatancy angle; however, this value only corresponds to a peak point of shear strength which reduces afterward as the shear deformation continues. Since the Mohr–Coulomb model cannot simulate such hardening–softening soil behavior and only considers perfect plasticity, a constant friction angle is adopted for all the simulations.

The results of the simulations are demonstrated in Fig. 13. It is evident that the variation of the ψ value in very small displacements (smaller than one meter) of the reverse fault does not have a dominant impact on the pipeline response and its effect appears at a larger amount of fault movement. In the larger fault displacement, the rise in the dilation angle has dominantly increased the maximum compressive strain, while this increasing trend is not observed for the maximum tensile strain. The pipeline is vulnerable to be damaged in compression (e.g., buckling mode of failure) even if the soil dilatancy is zero. Although the change in ψ value from 10° to 30° has not influenced the magnitude of maximum tensile strain, the pipeline in the soil with zero dilation angle has experienced a lower amount of tensile strain. As a brief, using soil with rounded particles as low-dilatancy materials around the pipeline only reduces the possibility of the tensile failure and it is not effective for the compressive failure mode.

5.5 Effect of the Burial Depth Ratio on Pipeline Response

To investigate the effect of burial depth to pipe diameter ratio (H/D) on the pipeline behavior, the response of an X65 steel pipeline ($D = 914.4$ mm and $t = 12.6$ mm) under big fault displacements (up to 4 m) is evaluated under various burial depths $H/D = 1.1$, 1.6, 1.9, and 2.7. Similarly, the benchmark sandy soil is considered for the analysis. The amount of maximum compressive and tensile strains caused in the pipeline is illustrated in Fig. 14. It is mentioned that it was not possible to read out proper tensile strains for some cases since there were very bad deformed geometries generated in the shallow buried pipelines for the fault displacements greater than 2 m. Totally, the deeper the pipeline is buried, the more the values of compressive and tensile strains are. The tensile strain values are considerably lower than the values of the compressive strain for a constant magnitude of the fault displacement. The maximum compressive strain of the pipelines exceeds the serviceability limit (corresponding to the damage from local buckling) at small fault displacements, while the tensile strain satisfies the limited value against the tensile failure even for the deep one ($H/D = 2.7$) at the fault displacement of 2 m.

The reason for the higher values of the strains is because of large and severe deformations generated in the pipeline according to Fig. 15. In other words, the low-depth pipelines experience a smaller amount of compressive and tensile strains since they can displace the upside soil largely, and therefore, lower frictional forces are applied to the pipeline from the surrounding soil.

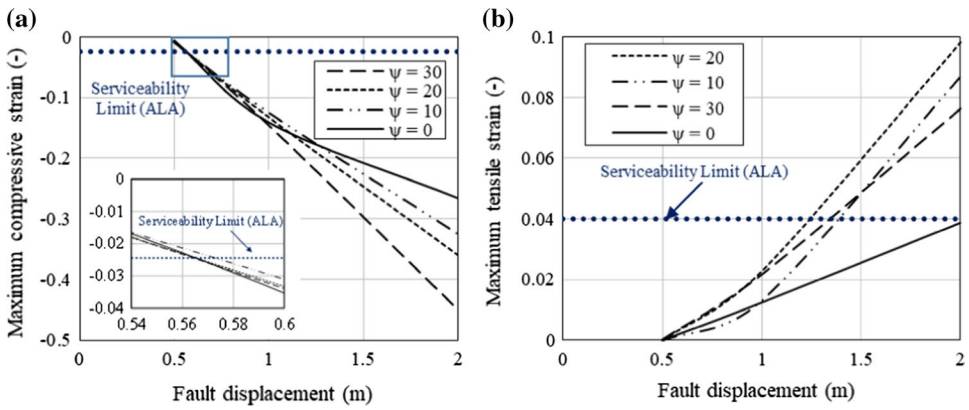

Fig. 13 The effect of dilation angle on the pipe strain **a** maximum compressive strain and **b** maximum tensile strain with fault displacement

5.6 Effect of Diameter-to-Thickness Ratio on Pipeline Response

To evaluate the effect of diameter-to-thickness ratio (D/t) on the pipeline response, various cases with $D/t = 36$, 48, 72, and 144 are considered here. A constant diameter $D = 914.4$ mm (36 in.) and various thickness $t = 6.35$ mm (0.25 in.), 12.7 mm (0.5 in.), 19.05 mm (0.75 in.) and 25.4 mm (1 in.) are chosen. The center of the pipeline is located at $H = 1.75$ m. The maximum tensile and compressive strains caused in the pipeline are shown in Fig. 16. As expected, the increase in the fault displacement causes to augment the maximum values of both tensile and compressive strains. For the thinnest pipe ($D/t = 144$), the strain variation is considerably sensitive to the fault displacement even for small fault displacements because for the current case, the wrinkling limit is very low $\varepsilon_c = 1.76\ t/D = -0.012$ and the pipeline exceeds this limit at very low values of fault displacement. At larger fault displacement, this variation is reduced because the pipe wall has been wrinkled.

The deformed shape of the pipelines for various D/t ratios is illustrated in Fig. 17. The deformation pattern of the pipeline is different for various D/t ratios. The pipeline with $D/t = 36$, i.e., the thickest pipe, has more vertical displacement compared to other D/t ratios. The increase in the wall thickness prevents the wrinkling phenomenon and instead, the pipe tends to experience beam buckling. This can be explained in such a way that the compressive forces

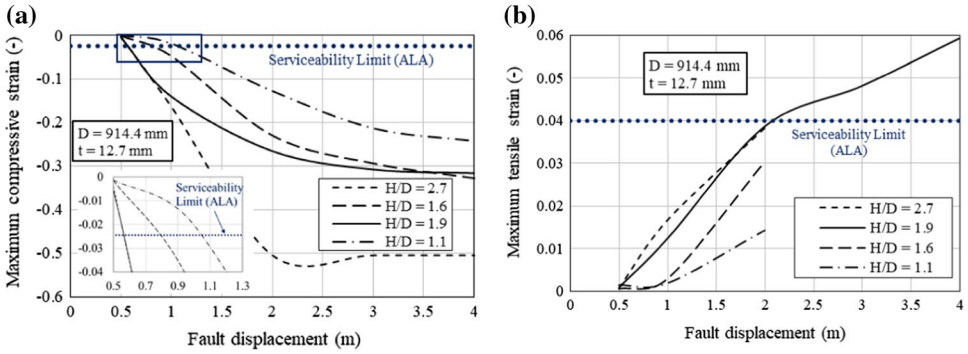

Fig. 14 The effect of burial depth to pipe diameter ratio (H/D) on the pipe strain with $D = 914.4$ mm and $t = 12.7$ mm **a** maximum compressive strain and **b** maximum tensile strain

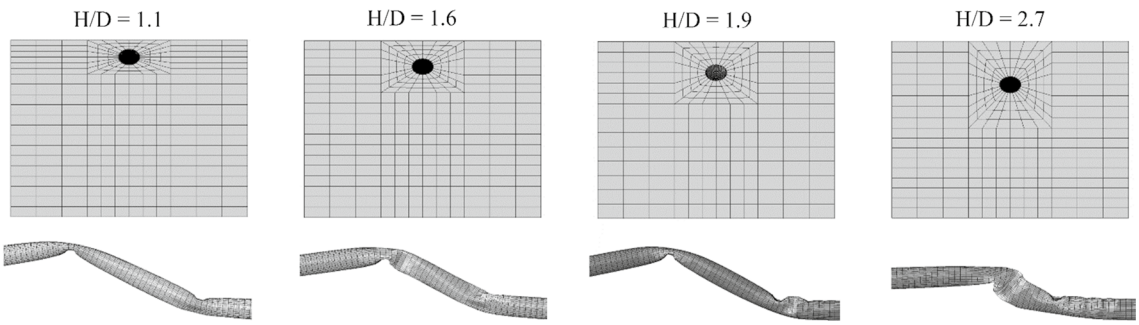

Fig. 15 Effect of the burial depth (H/D) on the pipeline deformation with $D = 914.4$ mm and $t = 12.7$ mm

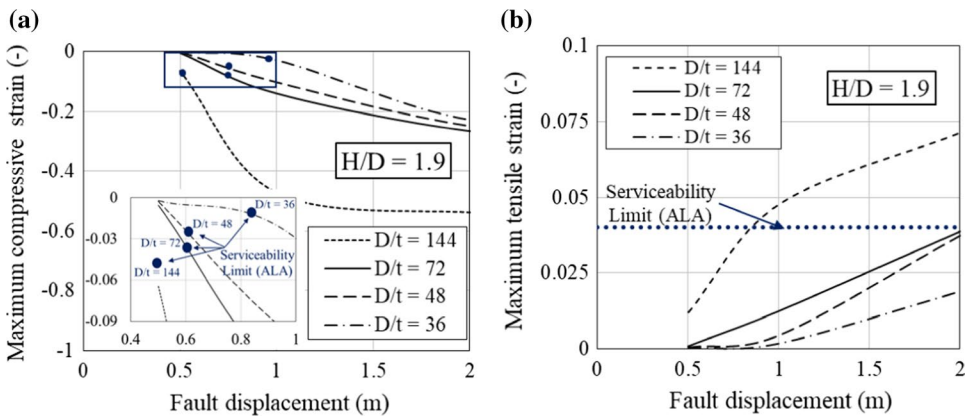

Fig. 16 The effect of diameter-to-thickness ratio (D/t) on the pipe strains with $H/D = 1.9$ **a** maximum compressive strain and **b** maximum tensile strain

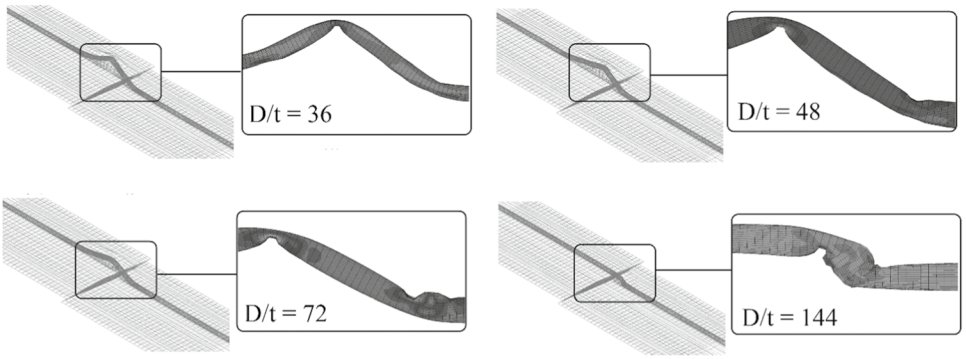

Fig. 17 Effect of the pipe thickness ratio (D/t) on the pipeline deformation with $H/D = 1.9$

are distributed over a large distance and therefore, a bigger length of the pipeline contributes to resistance against reverse fault movements. However, for the thicker pipelines ($D/t = 48$ and 72), the total displacement of the pipeline at the vicinity of the fault plane has decreased, which has resulted in the intensification of the strain at the buckled areas. For the high ratio of D/t (i.e., $D/t = 144$), the pipe cross-section could not withstand the forces caused in the pipeline, and therefore, the wrinkling phenomenon occurs in smaller fault displacement. Generally, the distance of the wrinkled location from the fault plane decreases as the D/t ratio increases.

Generally, the above parametric studies confirm that where less resistance is imposed by the surrounding soil to pipe, the pipeline's capacity has increased. This general rule is in good agreement with the recommendations of ASCE Guidelines [15] and EN 1998-4 [46] for the cases where the pipeline is crossing normal and strike-slip faults. It is noted that almost no direct case study has been done for a pipe across a reverse fault and it seems that no analytical approach is currently available for a pipe subjected to a reverse fault [9]. ASCE Guidelines [15] suggests using the finite element analysis in order to study the mechanical behavior of pipelines crossing reverse faults. Accordingly, based on the finite element analysis conducted in this paper, the following considerations are proposed to improve the capability of the pipeline to sustain differential movements of reverse fault:

1. Consistency and cohesion of stiff clays restrain pipeline deformation. This means that after the initiation of local buckling, severe distortion occurs at the fault-pipeline intersection point which results in high values of strain even in the low magnitude of fault displacement. Thus, to prevent excessive damages to the pipeline during the fault displacement, it is recommended to avoid the intersection of the pipeline route with the faults consisting of stiff clay.
2. In the cases where the intersection of the buried pipes/faults containing compacted and stiff soils is inevitable, it is required to replace the surrounding soil of the pipeline with loose and soft soils. This results in lower resistance forces in the contact surface between the soil and the pipe, which lessens the values of strains.
3. In large fault displacements, the rise in the dilation angle will increase the maximum compressive strain; therefore, it is not recommended to fill the surrounding zone of pipelines with dilative (i.e., mostly angular and granular) soils.
4. The reduction of the burial depth offers less resistance to pipe movement. It is therefore recommended to decrease the burial depth in the vicinity of faulting zones.
5. The pipeline's capacity to accommodate reverse fault offset can be increased significantly by choosing a thick-walled pipe. This is because the thick-walled pipe is more prone to experience beam buckling rather than local buckling.

6 Concluding Remarks

In this paper, a numerical study has been performed to investigate the behavior of the buried steel pipe against reverse fault motion. Unlike simplified beam-spring models, sophisticated 3-D continuum numerical models were employed here by using the finite element software ABAQUS. The complexity in the deformational behavior was taken into account in these analyses by considering elastoplastic material behavior for the soil and pipe with proper elements. The pipeline–soil interaction was simulated using automated surface-to-surface contact option provided by ABAQUS. The quasi-static condition of the fault displacement was also established in the analysis. The distortion of the pipeline cross-section and the pipe local buckling (or wrinkling phenomenon) were modeled using shell elements for the pipeline segment. The numerical approach was first validated by comparing the results with those of large-scale experimental tests. Then, this approach was compared with the simplified beam-spring approach to find out the advantage of the proposed

approach in the simulations of pipelines under reverse fault movement. As a parametric study, the effects of several geotechnical parameters and geometric conditions on the pipe response were investigated. From this study, the following conclusions are drawn:

1. The numerical approach proposed in this study can well capture the deformational behavior of buried pipelines where they cross reverse fault zones. It is possible to simulate the pipeline wrinkling phenomenon which is dominant for the pipelines crossing reverse faults. This distortion in the pipeline section cannot be considered by the simplified beam-spring modeling approach.
2. Local buckling (or wrinkling) mode is more sensitive to the pipeline failure rather than tensile failure mode in the case of crossing reverse faults. Based on the simulations, the value of compressive strain created in the pipeline is larger than that of the tensile strain because the pipeline is subjected to a combination of axial compression and bending.
3. The soil consistency has a great effect on the behavior of the buried pipeline for both cohesive and cohesionless soils. In numerical simulations, it seems that cohesion has a major effect on cohesive soils, while the friction angle has a significant role in the deformational behavior for cohesionless soils. Among the parameters, soil stiffness has the least effect.
4. The increase of the soil stiffness causes to decline in the imposed tensile strain slightly. However, it does not have a specific effect on the pipe compressive strain.
5. The increase of the soil dilation angle (ψ) resulted in the augmentation of the maximum compressive strain only in large fault displacements, while its effect on maximum tensile strain was almost negligible.
6. Based on the results of the numerical simulations in this study, it can be found out that the failed sections would be generated in the pipeline farther away from the fault plane as either the soil behaves more softly or the pipeline is more flexible.
7. Based on the results of this study, the pipeline capacity against failure can significantly be improved by reducing the burial depth (H/D) and the pipe thickness ratio (D/t) where it crosses a reverse fault zone.

Acknowledgements This research did not receive any specific Grant from funding agencies in the public, commercial, or not-for-profit sectors.

Compliance with Ethical Standards

Conflict of interest The authors declare that they have no conflict of interest.

References

1. Ariman, T.; Muleski, G.E.: A review of the response of buried pipelines under seismic excitations. Earthq. Eng. Struct. Dyn. **9**, 133–152 (1981)
2. Katayama, T.; Isoyama, R.: Damage to Buried Distribution Pipelines During the Miyagiken-Oki Earthquake. In: Proceedings of Recent Advances in Lifeline Earthquake Engineering in Japan, ASME California, pp. 97–104, (1980)
3. Kitaura, M.; Miyajima, M.: Damage to water supply pipelines. Soils Found. **36**, 325–333 (1996)
4. Liang, J.; Sun, S.: Site effects on seismic behavior of pipelines: a review. J. Press. Vessel Technol. **122**, 469–475 (2000)
5. O'Rourke, M.J.; Ayala, G.: Seismic damage to pipeline: case study. J. Transp. Eng. **116**, 123–134 (1990)
6. Ariman, T.: Buckling and rupture failure in pipelines due to large ground deformations. In: Wind and Seismic Effects: Proceedings of the 14th Joint Panel Conference of the US-Japan Cooperative Program in Natural Resources, US Dept. of Commerce, National Bureau of Standards,, pp. 259. (1983)
7. McCaffrey, M.; O'Rourke, T.: Buried pipeline response to reverse faulting during the 1971 San Fernando Earthquake. ASME Press. Vessels Pip. **77**(1983), 151–159 (1971)
8. Moradi, M.; Rojhani, M.; Galandarzadeh, A.; Takada, S.: Centrifuge modeling of buried continuous pipelines subjected to normal faulting. Earthq. Eng. Eng. Vib. **12**, 155–164 (2013)
9. O'Rourke, M.J.; Liu, X.: Response of buried pipelines subject to earthquake effects, MonographSeries, Multidisciplinary Center for Earthquake Engineering Research (MCEER) (1999)
10. Rojhani, M.; Moradi, M.; Galandarzadeh, A.; Takada, S.: Centrifuge modeling of buried continuous pipelines subjected to reverse faulting. Can. Geotech. J. **49**, 659–670 (2012)
11. Sun, S.: Earthquake damage to pipelines. In: Proceedings of 2nd U. S. National Conference on Earthquake Engineering, EERI, Stanford, pp. 61–67 (1979)
12. Towhata, I.: Geotechnical Earthquake Engineering. Springer, Berlin (2008)
13. Newmark, N.M.; Hall, W.J.: Pipeline Design to Resist Large Fault Displacement. In: Proceedings of U.S. National Conference on Earthquake Engineering, pp. 416–425. (1975)
14. Kennedy, R.; Chow, A.; Williamson, R.: Fault movement effects on buried oil pipeline. Transp. Eng. J. ASCE **103**(TE5), 617–633 (1977)
15. ASCE, Guidelines for the seismic design of oil and gas pipeline systems, committee on gas and liquid fuel lifelines, pp. 150–228. (1984)
16. Wang, L.R.L.; Yeh, Y.H.: A refined seismic analysis and design of buried pipeline for fault movement. Earthq. Eng. Struct. Dyn. **13**, 75–96 (1985)
17. Karamitros, D.; Bouckovalas, G.; Kouretzis, G.; Gkesouli, V.: An analytical method for strength verification of buried steel pipelines at normal fault crossings. Soil Dyn. Earthq. Eng. **31**, 1452–1464 (2011)
18. Karamitros, D.K.; Bouckovalas, G.D.; Kouretzis, G.P.: Stress analysis of buried steel pipelines at strike-slip fault crossings. Soil Dyn. Earthq. Eng. **27**, 200–211 (2007)
19. Abdoun, T.H.; Ha, D.; O'Rourke, M.J.; Symans, M.D.; O'Rourke, T.D.; Palmer, M.C.; Stewart, H.E.: Factors influencing the behavior of buried pipelines subjected to earthquake faulting. Soil Dyn. Earthq. Eng. **29**, 415–427 (2009)
20. Ha, D.; Abdoun, T.H.; O'Rourke, M.J.; Symans, M.D.; O'Rourke, T.D.; Palmer, M.C.; Stewart, H.E.: Centrifuge modeling of earthquake effects on buried high-density polyethylene (HDPE) pipelines crossing fault zones. J. Geotech. Geoenviron. Eng. **134**, 1501–1515 (2008)

21. O'Rourke, M.; Gadicherla, V.; Abdoun, T.: Centrifuge modeling of PGD response of buried pipe. Earthq. Eng. Eng. Vib. **4**, 69–73 (2005)
22. Hojat Jalali, H.; Rofooei, F.R.; Khajeh Ahmad Attari, N.: Performance of buried gas distribution pipelines subjected to reverse fault movement. J. Earthq. Eng. **22**, 1068–1091 (2018)
23. Jalali, H.H.; Rofooei, F.R.; Attari, N.K.A.; Samadian, M.: Experimental and finite element study of the reverse faulting effects on buried continuous steel gas pipelines. Soil Dyn. Earthq. Eng. **86**, 1–14 (2016)
24. Rofooei, F.R.; Jalali, H.H.; Attari, N.K.A.; Kenarangi, H.; Samadian, M.: Parametric study of buried steel and high density polyethylene gas pipelines due to oblique-reverse faulting. Can. J. Civ. Eng. **42**, 178–189 (2015)
25. Ariman, T.; Lee, B.-J.: Tension Bending Behavior of Buried Pipelines Under Large Ground Deformations in Active Faults. In: Lifeline Earthquake Engineering, ASCE, pp. 226–233. (1991)
26. Meyersohn, W.D.: Analytical and design considerations for the seismic response of buried piplines. Cornell University, Ithaca (1991)
27. Liu, X.; O'Rourke, M.J.: Behaviour of continuous pipeline subject to transverse PGD. Earthq. Eng. Struct. Dyn. **26**, 989–1003 (1997)
28. Far, M.S.: Discussion of "a semi-empirical model for peak strain prediction of buried X80 steel pipelines under compression and bending at strike-slip fault crossings" by Liu et al. (2016). J. Nat. Gas Sci. Eng. **52**, 432–433 (2018)
29. Liu, X.; Zhang, H.; Han, Y.; Xia, M.; Zheng, W.: A semi-empirical model for peak strain prediction of buried X80 steel pipelines under compression and bending at strike-slip fault crossings. J. Nat. Gas Sci. Eng. **32**, 465–475 (2016)
30. Takada, S.; Hassani, N.; Fukuda, K.: A new proposal for simplified design of buried steel pipes crossing active faults. Earthq. Eng. Struct. Dyn. **30**, 1243–1257 (2001)
31. Trifonov, O.V.: Numerical stress–strain analysis of buried steel pipelines crossing active strike-slip faults with an emphasis on fault modeling aspects. J. Pipeline Syst. Eng. Pract. (2014)
32. Trifonov, O.V.; Cherniy, V.P.: Elastoplastic stress–strain analysis of buried steel pipelines subjected to fault displacements with account for service loads. Soil Dyn. Earthq. Eng. **33**, 54–62 (2012)
33. Vazouras, P.; Karamanos, S.A.; Dakoulas, P.: Finite element analysis of buried steel pipelines under strike-slip fault displacements. Soil Dyn. Earthq. Eng. **30**, 1361–1376 (2010)
34. Vazouras, P.; Karamanos, S.A.; Dakoulas, P.: Mechanical behavior of buried steel pipes crossing active strike-slip faults. Soil Dyn. Earthq. Eng. **41**, 164–180 (2012)
35. Xie, X.; Symans, M.D.; O'Rourke, M.J.; Abdoun, T.H.; O'Rourke, T.D.; Palmer, M.C.; Stewart, H.E.: Numerical modeling of buried HDPE pipelines subjected to strike-slip faulting. J. Earthq. Eng. **15**, 1273–1296 (2011)
36. Zhang, J.; Liang, Z.; Han, C.: Buckling behavior analysis of buried gas pipeline under strike-slip fault displacement. J. Nat. Gas Sci. Eng. **21**, 921–928 (2014)
37. González, O.; Fraile, A.; Hermanns, L.: A numerical and semi-analytical comparison for structural analysis of fault-crossing pipelines. Comptes Rendus Mécanique **343**, 397–409 (2015)
38. Joshi, S.; Prashant, A.; Deb, A.; Jain, S.K.: Analysis of buried pipelines subjected to reverse fault motion. Soil Dyn. Earthq. Eng. **31**, 930–940 (2011)
39. Liu, X.; Zhang, H.; Li, M.; Xia, M.; Zheng, W.; Wu, K.; Han, Y.: Effects of steel properties on the local buckling response of high strength pipelines subjected to reverse faulting. J. Nat. Gas Sci. Eng. **33**, 378–387 (2016)
40. ABAQUS, Abaqus v6. 12 Documentation-ABAQUS analysis user's manual, Abaqus, Providence, RI, (2012)
41. Guidelines for the design of buried steel Pipe American Lifelines Alliance—ASCE, July 2001 (with addenda through February 2005)
42. Ramberg, W.; Osgood, W.R.; U.S.N.A.C.F. Aeronautics: Description of Stress–Strain Curves by Three Parameters, National Advisory Committee for Aeronautics, (1943)
43. Savidis, S.A.; Schepers, W.; Nomikos, E.; Papadakos, G.: Design of a natural gas pipeline subject to permanent ground deformation at normal faults: a parametric study on numerical VS. Semi-Anal. Proced. Santiago **10**, 13 (2011)
44. IITK-GSDMA, Guidelines for seismic design of buried pipelines. In: National Information Center of Earthquake Engineering, Indian Institute of Technology Kanpur (2007)
45. C.S. Association, Oil and Gas Pipeline Systems-CSA Z662-15, CSA Group (2015)
46. EN 1998-4: Eurocode 8: Design of structures for earthquake resistance—part 4: Silos, tanks and pipelines. In: CEN European Committee for Standardisation (2006)
47. Liu, B.; Liu, X.; Zhang, H.: Strain-based design criteria of pipelines. J. Loss Prev. Process Ind. **22**, 884–888 (2009)
48. Whidden, W.R.: Buried flexible steel pipe: design and structural analysis. In: American Society of Civil Engineers, (2009)
49. Kong, L.; Zhou, X.; Chen, L.; Shuai, J.; Huang, K.; Yu, G.: True stress–strain curves test and material property analysis of API X65 and API X90 gas pipeline steels. J. Pipeline Syst. Eng. Pract. **9**, 04017030 (2018)
50. Specification, API.: 5L, Specification for Line Pipe, Edition March, (2004)
51. Sreenath, S.; Saravanan, U.; Kalyanaraman, V.: Beam and shell element model for advanced analysis of steel structural members. J. Constr. Steel Res. **67**, 1789–1796 (2011)
52. Sarawit, A.; Kim, Y.; Bakker, M.; Peköz, T.: The finite element method for thin-walled members-applications. Thin-walled Struct. **41**, 191–206 (2003)